Contents lists available at ScienceDirect

Surfaces and Interfaces

journal homepage: www.sciencedirect.com/journal/surfaces-and-interfaces

The role and effect of CdS-based TiO$_2$ photocatalysts enhanced with a wetness impregnation method for efficient photocatalytic glucose electrooxidation

Aykut Caglar [a], Nahit Aktas [a,b,*], Hilal Kivrak [b,c,d,**]

[a] Department of Chemical Engineering, Van Yuzuncu Yil University, Van, Turkey
[b] Department of Chemical Engineering, Kyrgyz-Turkish Manas University, Bishkek, Kyrgyzstan
[c] Department of Chemical Engineering, Eskisehir Osmangazi University, Eskişehir, Turkey
[d] Translational Medicine Research and Clinical Center, Eskisehir Osmangazi University, Eskişehir, Turkey

ARTICLE INFO

ABSTRACT

The 0.1% CdS-based TiO$_2$photocatalysts with different atomic ratios were synthesized by the wetness impregnation (WI) method. These photocatalysts were characterized to actively determine surface area using TPx analyses (TPR, TPO, and TPD). Furthermore, surface structures and properties of photocatalysts were defined by analyses such as XRD, UV–VIS spectroscopy, SEM-EDX and mapping, fluorescence spectroscopy, TEM-EDS, and XPS. The photocatalytic activities of photocatalysts were examined by CV, CA, and EIS electrochemical analyses to investigate use in photocatalytic fuel cells (PFCs) in glucose solution in the dark and under UV illumination. The characterization analyses revealed that anatase TiO$_2$ formed in the catalyst and its electronic structure and surface properties changed when doped with metal. The photocatalytic glucose electrooxidation (PGE) results indicated that the 0.1% CdS(50-50)/TiO$_2$ catalyst exhibited much higher photocatalytic activity, stability, and resistance than other catalysts both in the dark (5.21 mA/cm^2) and under UV illumination (16.21 mA/cm^2). The study offers a promising new type of photocatalyst for PFC applications.

1. Introduction

Recently, the demand for energy has increased with the growth of industry and the increase in the population. The world's energy needs are met by fossil fuel sources such as oil, coal, and natural gas [1]. These energy resources have the disadvantages of limited use and the formation of harmful gases for the environment such as CO$_2$, SO$_x$, and NO$_x$. Therefore, researchers have turned to alternative energy sources. Alternative energy sources have been examined in many fields such as water splitting [2], hydrogen storage [3], supercapacitors [4], solar energy [5], lithium-ion batteries [6], and fuel cells [7] in the literature. Fuel cells have attracted the attention of the scientific world among these alternative energy sources as clean energy sources to meet the world's energy demand and will be one of the most important energy sources in the future. Fuel cells promise to be sustainable and efficient energy sources for a clean future that converts chemical energy directly into electrical energy [8,9]. Photocatalytic fuel cells (PFCs) containing semiconductor photoanode, cathode, and electrolyte such as methanol [10], ethanol [11], and glucose (C$_6$H$_{12}$O$_6$) [12] are up-and-coming devices that could meet energy needs and prevent environmental pollution by utilizing sunlight as energy input. Glucose is a high energy density (4.43 kWh/kg), non-toxic, flammable and non-volatile, potential hydrogen carrier and is the most abundant simple sugar in nature [13–17]. A glucose molecule can produce 24 electrons and yield -2870 kJ/mol of energy via the complete oxidation to CO$_2$. It is worth noting that glucose consists mostly of gluconic acid and a two-electron generating system in all studies to date [18].

Anode : C$_6$H$_{12}$O$_6$ + 24OH$^-$ → 6CO$_2$+ 12H$_2$O + 24e$^-$ (1)
Cathode : 6O$_2$ + 24e$^-$ + 12H$_2$O → 24OH$^-$ (2)
Overall :C$_6$H$_{12}$O$_6$ + 6O$_2$ → 6CO$_2$ + 6H$_2$O (3)
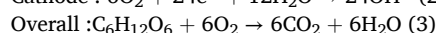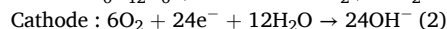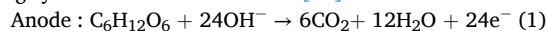
The catalytic oxidation of glucose was widely explored as a renewable energy source to meet energy demands. Metal, metal oxide nanoparticles, enzymes, and semiconductor materials are widely used in this oxidation system [19]. Photocatalysis changes the rate of a chemical
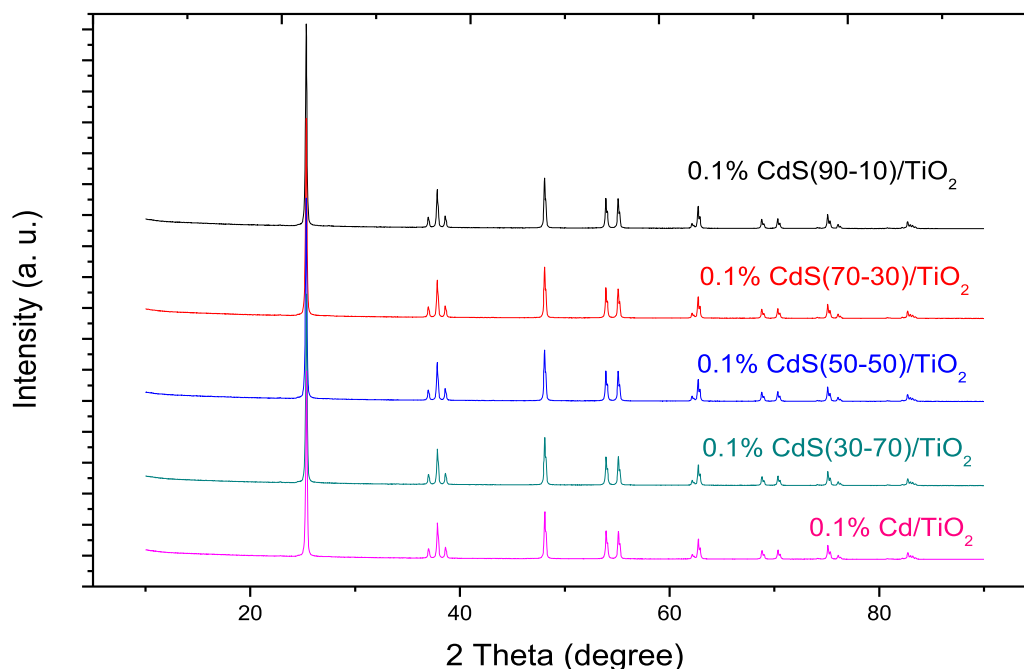
Fig. 1. XRD patterns of 0.1% Cd/TiO$_2$ and 0.1% CdS-doped TiO$_2$ catalysts.

reaction when a semiconductor material is exposed to light. Semiconductor materials are photocatalysts that absorb light and behave as catalysts for chemical reactions [20]. Semiconductor materials such as titanium dioxide (TiO$_2$), zinc oxide (ZnO), and tin dioxide (SnO$_2$) are used as photocatalysts in the literature [21–25]. TiO$_2$ (3.2 eV wide band gap [26]), which was first discovered by Fujishima and Honda in 1972 with its water separation feature, was used as a photoanode [27].

TiO$_2$ has the disadvantage that it adsorbs less than 5% of the solar source of UV light and causes rapid recombination of photogenerated electron-hole pairs, leading to low quantum yield and activity for PFCs. Researchers have studied TiO$_2$-based metals [28], metal sulfides [29], metal oxides [30], and carbon-based materials [31] to improve their photocatalytic activities for use in PFCs. Hu et al. [32] reported that they investigated the effects of photocatalytic degradation mechanisms of different organic classes and comprehensive characterization of photoelectrochemical properties by optimization of TiO$_2$, WO$_3$ and Nb$_2$O$_5$ photoanodes with statistical 2k factorial design for PFCs. They emphasized that the TiO$_2$-based PFC provided the highest photocurrent density as a result of its high intrinsic quantum efficiency compared to the others. Kivrak et al. [33] reported photocatalytic methylene blue degradation and electrooxidation of Cd/TiO$_2$ catalyst. Ozok-Arici et al. [34] examined the catalytic activity of Pd-doped organic catalyst for glucose electrooxidation. They emphasized that the catalyst had high catalytic activity of 0.57 mA/cm^2. In addition, few layer graphene/ITO (6.58 mA/cm^2) [14], N-doped few layer graphene/ITO (9.12 mA/cm^2) [15], CNT/nano-TiO$_2$/Pt complex electrode (13 mA/cm^2) [35], Pt-graphene/ITO (9.21 mA/cm^2), NiO-TiO$_2$-ZrO$_2$/SO$_4^{2-}$ (5.19 mA/cm^2) [36], Cu/Cu$_2$O/TNT (6.40 mA/cm^2) [37], and Ni(OH)$_2$-24.2%/TNT (23.43 mA/cm^2) [38] materials were studied for glucose electrooxidation in the literature. Photocatalytic performances of semiconductor materials such as TiO$_2$ with different metals were investigated in many areas such as decomposition, hydrogen production, and CO$_2$ reduction [39,40]. Moreover, it is known that metal loading on the support plays an important role in determining the catalytic activity of catalysts in photocatalytic fuel cells. The metal loading on the support and the amount of metal affecting the thickness of the fuel cell catalyst layer also impact the cell performance. Literature studies investigated the close relationship between metal loading, particle size, and catalyst layer thickness on the support and their effect on

fuel cell performance. High metal loading on the support material reduces the interparticle distance, which affects the catalytic activity. Furthermore, the catalyst causes a decrease in surface area, thus leading to a decrease in catalytic activity [41,42].

Although there are many photocatalytic studies, photocatalytic electrooxidation studies about photoanode catalysts for fuel cells are not available in the literature, except for a few studies. In the present study, CdS-based TiO$_2$photocatalysts were synthesized at different atomic molar ratios (90:10, 70:30, 50:50, 30:70) by utilizing the wetness impregnation (WI) method. The reduction process was realized in a furnace under argon gas at 400 °C. The structure of photocatalysts was characterized by using the XRD, SEM-EDX and mapping, TEM, XPS, UV-VIS spectroscopy, fluorescence spectroscopy, TPR, TPO, and TPD analyses. The CV, CA, and EIS analyses were performed to examine the catalytic activity for photocatalytic glucose electrooxidation (PGE) in the dark and under UV illumination.

2. Experimental

2.1. Synthesis of CdS-based TiO$_2$ catalysts

All chemicals were bought from Sigma-Aldrich. CdS-based TiO$_2$ catalysts were synthesized with different ratios by using the WI method. Catalysts prepared by the WI method do not generally produce highly dispersed particles due to the absence of induced interaction between the metal precursor and the support, which allows mobility of the precursor during drying. In addition, the WI method provides a great advantage of more easily preparing an active substance layer on the catalyst surface compared to other methods [43,44]. Firstly, the appropriate amounts of Cd precursor and sulfur were distributed under sonication in DI water in a beaker for CdS-based TiO$_2$ catalysts. After the metal precursors were homogeneously dispersed in DI water, TiO$_2$ was added and mixed for 30–60 min with the help of a glass rod. This was then left to dry at 85 °C overnight. Finally, the reduction process for the obtained catalysts was completed by keeping them under argon gas for 2 h at up to 400 °C with a heating rate of 10 °C/min in a furnace. Cooling was carried out with the help of a fan. The 0.1% CdS-based TiO$_2$ catalysts were synthesized under the same synthesis conditions with 90-10, 70-30, 50-50, and 30-70 metal ratios.
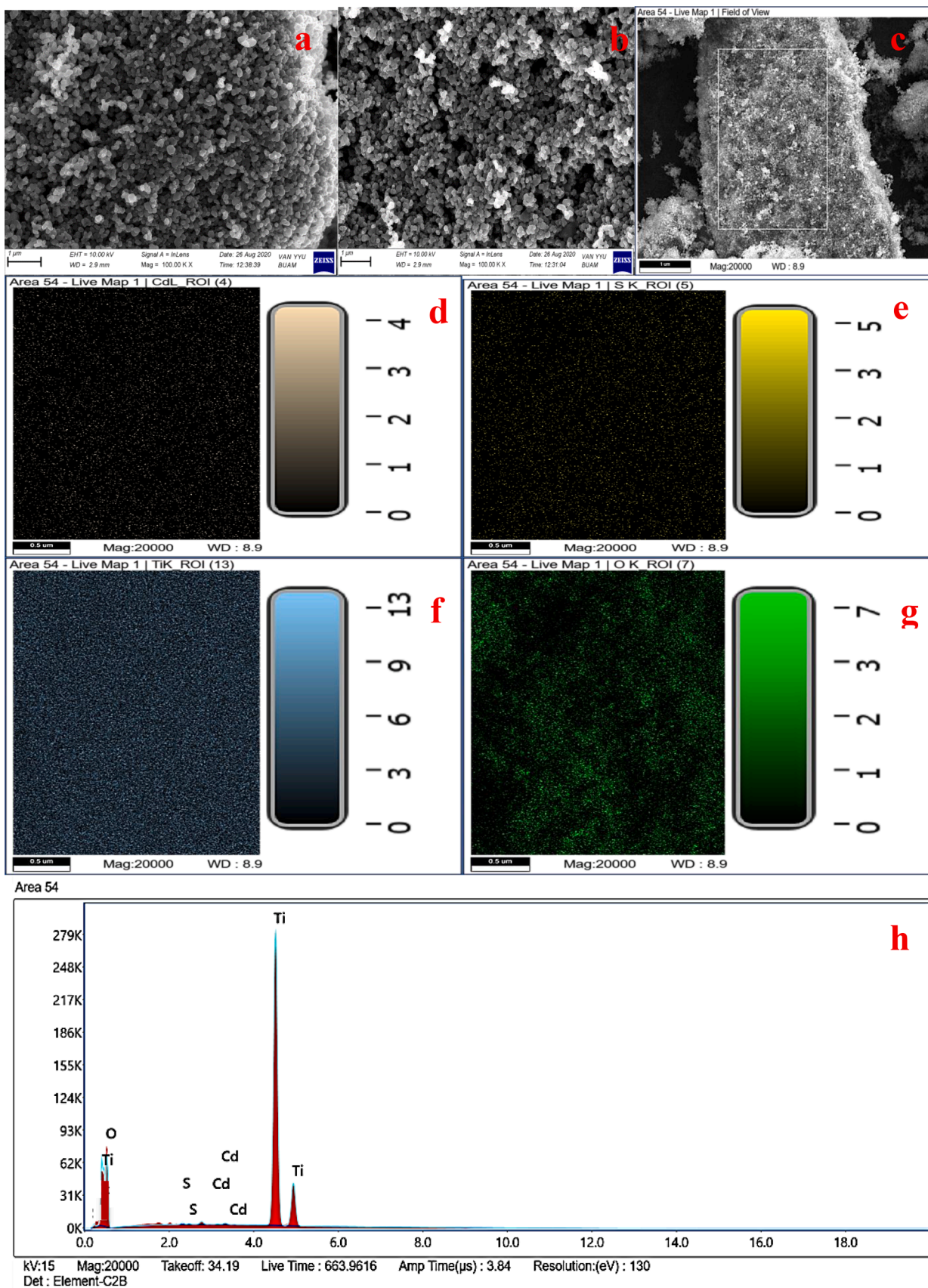
Fig. 2. SEM images (a–c), EDX (h), and mapping (Cd (d), S(e), Ti (f), O (g)) of 0.1%CdS(50-50)/TiO$_2$catalyst.

Table 1
Weight elemental composition of CdS-based TiO_2 catalysts.

Elements (%)	Samples			
	0.1% CdS(90-10)/ TiO_2	0.1% CdS(70-30)/ TiO_2	0.1% CdS(50-50)/TiO_2	0.1% CdS(30-70)/TiO_2
Cd	0.06	0.10	0.13	0.09
S	0.14	0.15	0.17	–
Ti	69.11	71.32	76.79	72.12
O	30.69	28.43	22.91	27.79

2.2. Characterization of CdS-based TiO_2 catalysts

The X-ray diffraction (XRD) patterns were used to examine crystal structures with an Empyrean (PANanalytical) diffractometer. The surface morphologies of catalysts were characterized by utilizing SEM-EDX and mapping (ZEISS Sigma 300) analysis. TEM analysis was obtained using a Hitachi HighTech HT7700 device at 120 kV accelerating voltage and a maximum resolution of 0.204 nm. UV–VISspectra were recorded by utilizing the Shimadzu UV-3600 Plus device. The fluorescence spectrum of the photocatalysts was measured with a Perkin Elmer FL6500fluorescence spectrophotometer. The elemental composition and oxidation state of the 0.1% CdS(50-50)/TiO_2 catalyst were examined using XPS analysis (Specs-Flex) with a CCD detector (Kα (Al): 1486.7 eV). Micromeritics Chemisorb 2750 equipment was used to examine H_2-TPR, O_2-TPO, and NH_3-TPD analyses with an automated system linked to ChemiSoft TPx software.

2.3. Photo-electrochemical measurements

The CV, CA, and EIS electrochemical analyses of the catalysts were completed using a potentiostat device to investigate activity, stability, and resistance, respectively. All analyses were performed in a three-electrode system with a scan rate of 100 mV/s in 1 M KOH + 0.5 $C_6H_{12}O_6$ solution. These three electrodes, which are the reference electrode, the working electrode, and the counter electrode, were Ag/AgCl, titanium metal, and Pt wire, respectively. A catalyst slurry was obtained by mixing CdS-based TiO_2 catalysts and nafion and it was transferred onto titanium metal with 0.5 cm^2 area.The CV, CA, and EIS analyses were used to investigate the catalytic activities of PGEin the dark and under UV illumination. The UV lamp used for illumination had a power of 366 nm (long wavelength) and 6 W placed in a cabinet connected to the UVP device.

3. Results and discussion

3.1. Physical characterization

Fig. 1 presents the XRD patterns of CdS-doped TiO_2 catalysts. The diffraction peaks at around 2Ө for 25.32°, 36.92°, 37.70°, 38.70°, 47.98°, 53.91°, 55.20°, 62.67°, 68.86°, 70.40°, 75.02°, and 82.78° correspond to (101), (103), (004), (112), (200), (105), (211), (204), (116), (220), (215), and (224) crystal planes of TiO_2 anatase, respectively (JCPDS: 21-1272) [45,46]. All the diffraction peaks in the XRD models appeared to describe the TiO_2 anatase phase well. However, there were no characteristic peaks for CdS due to the low metal amount in CdS-doped TiO_2 catalysts [47]. When the structural properties of metal-doped TiO_2 were examined by XRD analysis in the studies in the literature, it was emphasized that the peak did not occur due to the low amount of metal and it was well distributed in TiO_2 [48].

The SEM-EDX and mapping analyses were performed to observe the surface morphology of the CdS-doped TiO_2 catalyst. Fig. 2(a–h) illustrates SEM images, EDX analysis, and mapping of the catalyst. Due to the low amount of metal used during the synthesis compared to TiO_2, SEM images mostly showed TiO_2 structures. This demonstrates that the

metals did not agglomerate and are well dispersed. Cd, S, Ti, and O metals were illustrated in EDX and mapping analysis. According to the EDX analysis results, the existence of cadmium and sulfur was observed in all CdS-based TiO_2 catalysts (Table 1 and Fig. 2j). From Table 1 and Fig. 2j, it was observed that Cd and S metals were composed of different ratios in the EDX analysis. In addition, the formation of CdS-based TiO_2 catalyst obtained by mapping analysis formed green, turquoise, yellow, and brown particles which indicate the presence of O, Ti, S, and Cd, respectively (Fig. 2d–g).

TEM analysis was used to examine the particle size, size distribution, and morphology of the materials. The TEM images of 0.1% CdS(50-50)/TiO_2 catalyst are given in Fig. 3(a–i). In addition, EDX analysis and particle size distribution were performed for the catalyst. From Fig. 3 (a–g), the particles did not agglomerate and were generally homogeneously dispersed. TiO_2 structures have larger particle size, while CdS metal particles have distributed and smaller particle size [49].The histogram and particle size of the 10 nm image are given in Fig. 3h. Particle size was about 5.1 nm. In many studies, it was emphasized that the activity increased with the reduction in particle size [50,51]. EDX results revealed the presence of Cd, S, Ti, and O particles. This result is equivalent to the SEM-EDX results.

Fig. 4(a–e) presents the possible chemical states of Cd and S in the 0.1% CdS(50-50)/TiO_2 catalyst defined by using XPS analysis. In all XPS results, peak positions were determined relative to C 1s at a binding energy of 284.6 eV. The general spectrum for XPS analysis (Fig. 4a) of the 0.1% CdS(50-50)/TiO_2 catalyst indicates peaks at C 1s, Ti 2p, O 1s, Cd 3d, and S 2p. The C 1s peak has three different chemical shift components with the binding energy of 284.2, 284.8, and 285.8 eV and could be attributed to C–C, C=C, and C-O or C–OH [52,53]. From Fig. 4c, the Ti 2p spectra at binding energy about 458.6 eV and 464.4 eV were composed of Ti $2p_{3/2}$ and Ti $2p_{1/2}$ peaks, showing the presence of Ti^{4+} in TiO_2 lattice [54]. The binding energy at 405.2 eV and 412.0 eV for Cd 3d (Fig. 4d) has two peaks at $3d_{5/2}$ and $3d_{3/2}$, which shows the possible formation of CdO and is consistent with the values noted for Cd^{2+} [55,56]. The difference between the binding energies of the Cd $3d_{5/2}$ and Cd $3d_{3/2}$ peaks was found to be approximately 6.8 eV. This difference confirms the presence of characteristic +2 Cd 3d states on the sample surface [57]. In addition, this difference was 7 eV for Cd/TiO_2 catalyst in the literature [58]. The shifts in energy levels of Cd and S elements from XPS core level results show that their electronic states differ. Fig. 4e demonstrates the binding energies of S 2p. The basic peaks of S 2p were located at 160.4 eV and 163.8 eV for $2p_{3/2}$ and $2p_{1/2}$, corresponding to S^{2-}, respectively. Furthermore, binding energy at 167.8 eV could be attributed to the presence of an S–O bond [59]. The measured atomic concentrations and probable chemical states of C 1s, Ti 2p, O 1s, Cd 3d, and S 2p for the 0.1% CdS(50-50)/TiO_2 catalyst are summarized in Table 2. As can be seen from Table 2, the desired metals in the catalyst structure were formed. The atomic ratios between Cd and S are close to each other (43-57), a value close to the atomic ratio of the catalyst (50-50), as was planned. In addition, the chemical bonding states and peaks in binding energies of Cd, S, Ti, and O metals in the 0.1% CdS(50-50)/TiO_2 catalyst indicate that the desired catalyst structure was formed.

The optical properties, one of the most important parameters for the photocatalytic activity of the TiO_2 and CdS-based TiO_2 catalysts, were characterized by utilizing a UV-visible diffuse reflectance spectrum in the region of 300−800 nm. Fig. 5a and b indicate the UV-VIS absorbance spectra and the Tauc plots, respectively. As depicted in Fig. 5a, TiO_2 displayed strong absorption under ultraviolet light with a wavelength at about 400 nm due to the band-gap of anatase-TiO_2. The preparation of TiO_2 with Cd and CdS metals targeted a change in the band-gap while remaining in the UV region and an increase the catalytic activity. Fig. 5a demonstrates that the absorption spectrum of CdS-based TiO_2 stretched from 402 nm, respectively. As shown from Tauc plots in Fig. 5b, the band gap energies of the TiO_2 and CdS-based TiO_2 catalysts obtained from the formula λ = 1240/Eg were 3.25 eV and 3.20 eV, respectively.
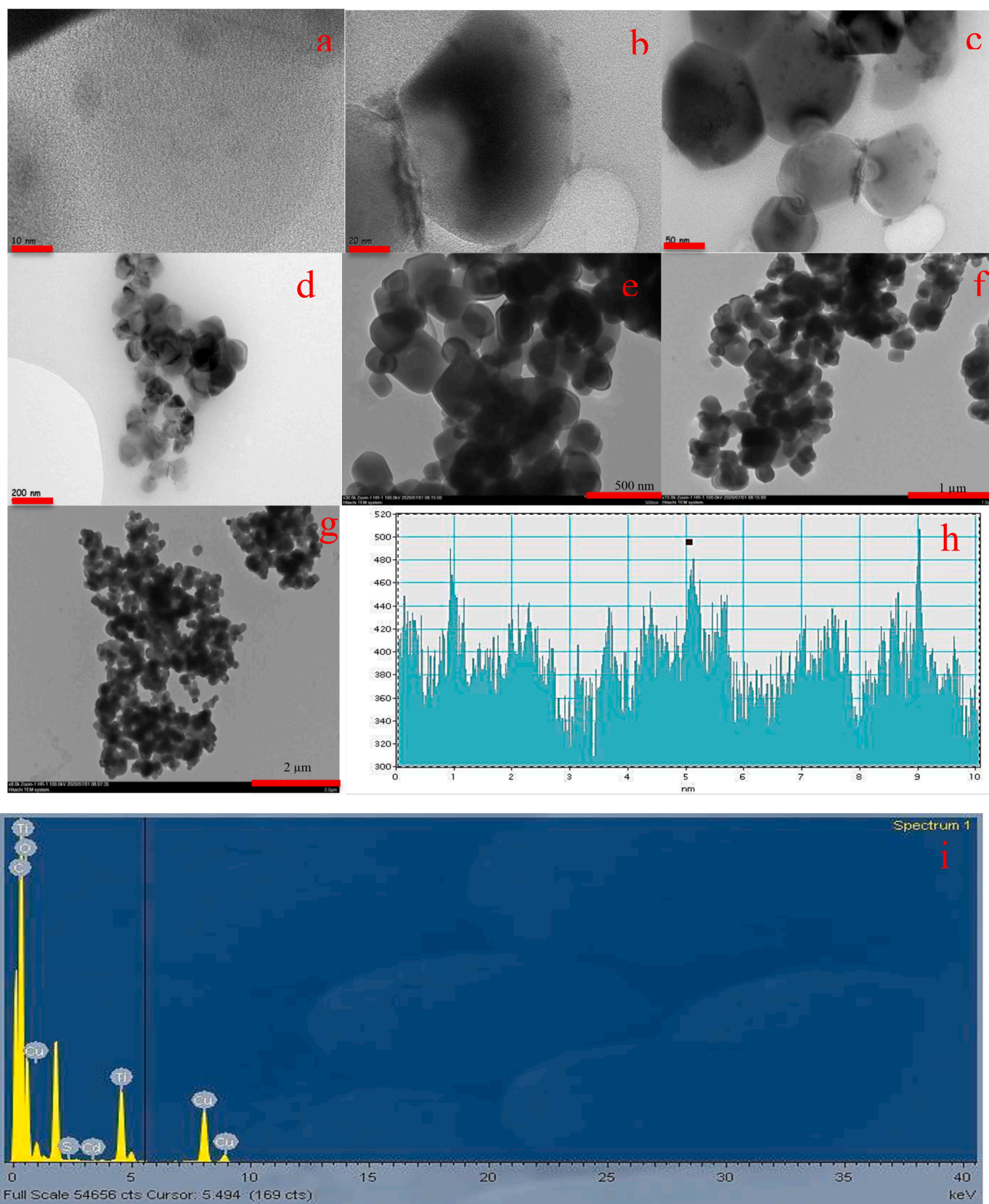
Fig. 3. TEM images of 0.1% CdS(50-50)/TiO$_2$ catalyst (a) 10 nm, (b) 20 nm, (c) 50 nm, (d) 200 nm, (e) 500 nm, (f) 1 μm, (g) 2 μm (h) particle size histogram (10 nm), and (i) EDS analysis.
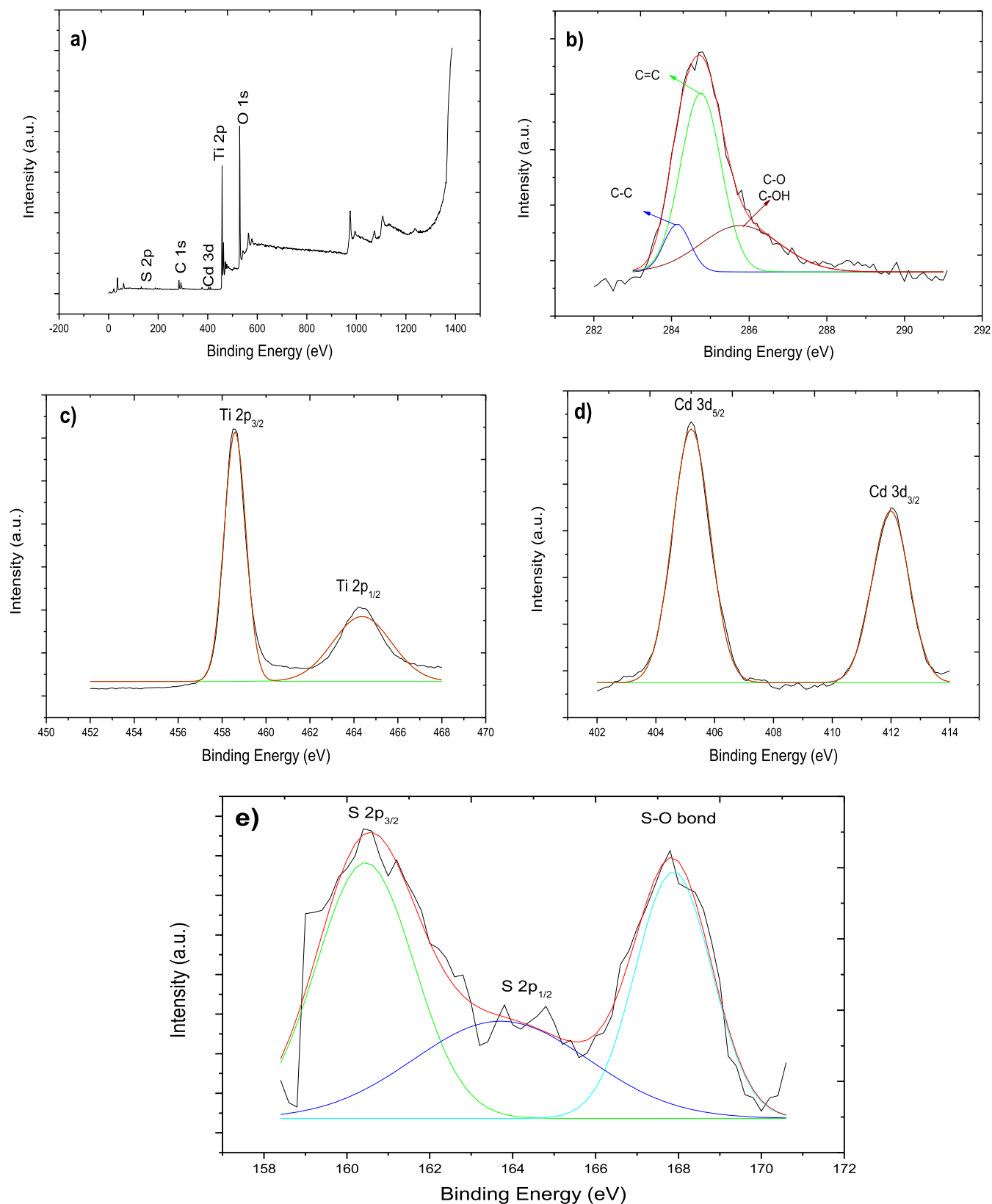
Fig. 4. XPS spectra of (a) general spectrum (b) C 1s, (c) Ti 2p, (d) Cd 3d, (e) S 2p for 0.1% CdS(50-50)/TiO$_2$ catalyst.

These band-gap results show that the introduction of CdS into the TiO$_2$ structure results in an increase in the ability to absorb light [64]. The junction between semiconductors and metals are heterostructures based on doping of metallic nanoparticles on crystalline semiconductors. Such

doping can inhibit electron/hole recombination by sequestering photoelectrons from the conduction band of the semiconductor to the surface of metallic nanoparticles (Fig. 5c). TiO$_2$ fermi levels are lower than CdS. Under UV illumination, valence band (VB) electrons excite the

Table 2

Curve fitting and probable chemical states of the XPS spectra for C1s, Ti2p, Cd3d, and S2p regions.

Name	Start BE	Peak BE	End BE	FWHM (eV)	Area	At. %	BE (eV)	Possible chemical state	Relative intensity %	Refs.
							284.2	C-C	25.73	
C 1s	283.0	284.6	288.6	2.136	2747.0	11.271	284.8	C=C	48.70	[52,53]
							285.8	C-O	25.57	
O 1s	526.2	530.0	538.0	2.147	44,439.4	62.233	–	–	–	
Ti 2p$_{3/2}$	456.3	458.6	467.7	1.549	26,409.2	20.759	458.6	Ti^{4+}	76.90	[60]
							464.4	Ti^{4+}	23.10	[61]
Cd 3d$_{5/2}$	403.2	405.2	413.9	2.389	864.3	0.296	405.2	Cd^{2+}	53.88	[62]
							412.0	Cd^{2+}	46.12	[63]
							160.4	S^{2-}	33.58	
S 2p	158.8	161.4	167.4	2.612	163.6	0.399	163.8	S^{2-}	32.88	[59]
							167.8	S-O bond	33.54	
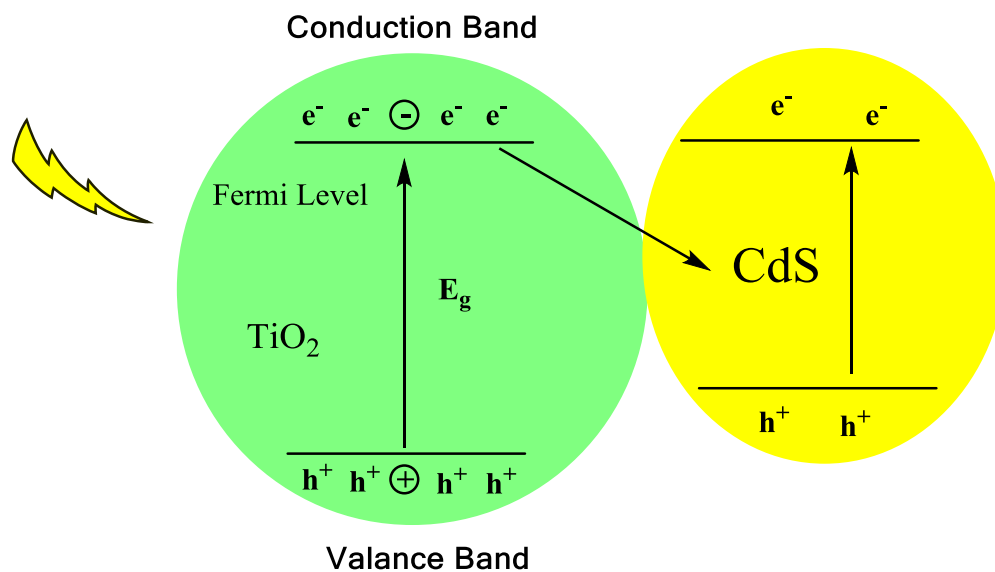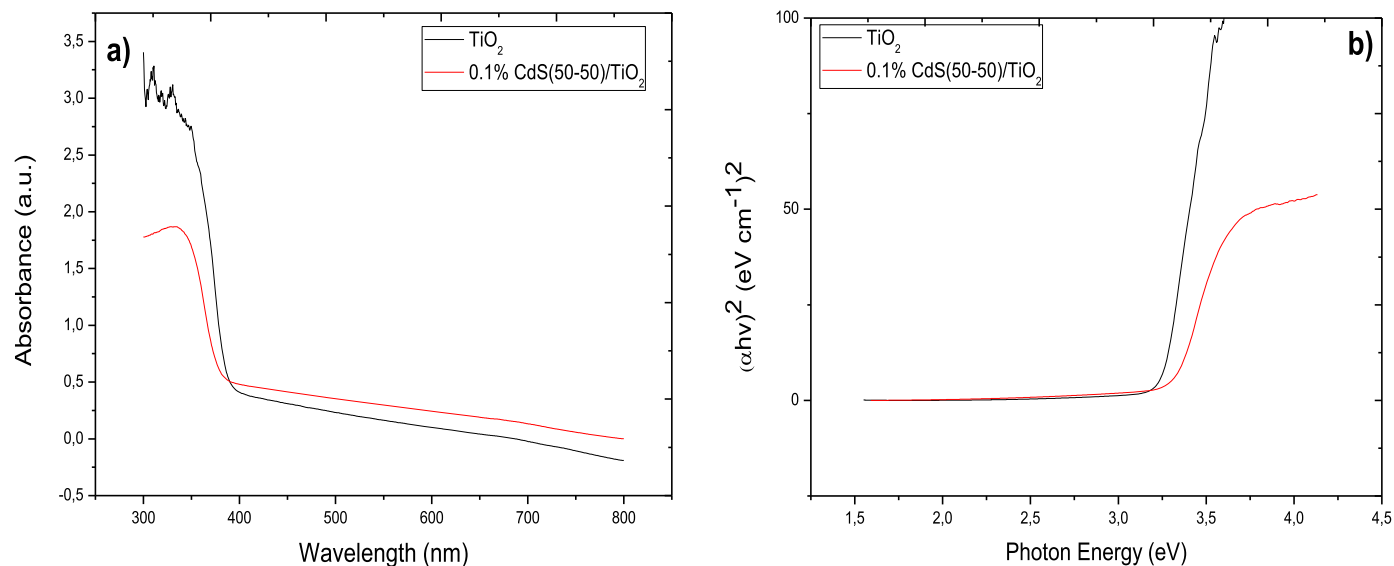
Fig. 5. (a) UV-VIS absorbance spectrum, (b) Tauc plots, and (c) schematic of the band gap for TiO$_2$ and 0.1% CdS(50-50)/TiO$_2$ catalysts.

conduction band (CB) of TiO$_2$ and CdS. The photogenerated electrons in TiO$_2$ CB easily move to the CdS VB and recombine with the holes in CdS VB due to the electric field force at the interface [65]. Furthermore, the addition of CdS into TiO$_2$ shows that it can effectively improve the absorption of UV light for catalytic activity.

The fluorescence spectrum of TiO$_2$ and 0.1% CdS(50-50)/TiO$_2$ catalysts is presented in Fig. 6a and b. Thanks to this spectrum, the photocatalytic activity efficiency of the catalysts and the charge capturing properties in the semiconductor can be determined [66]. In Fig. 6, the peak density at approximately 363 nm, 377 nm, and 663 nm for 0.1% CdS(50-50)/TiO$_2$ catalyst was weaker than TiO$_2$. Fluorescence emission in semiconductor materials is mainly due to the recombination
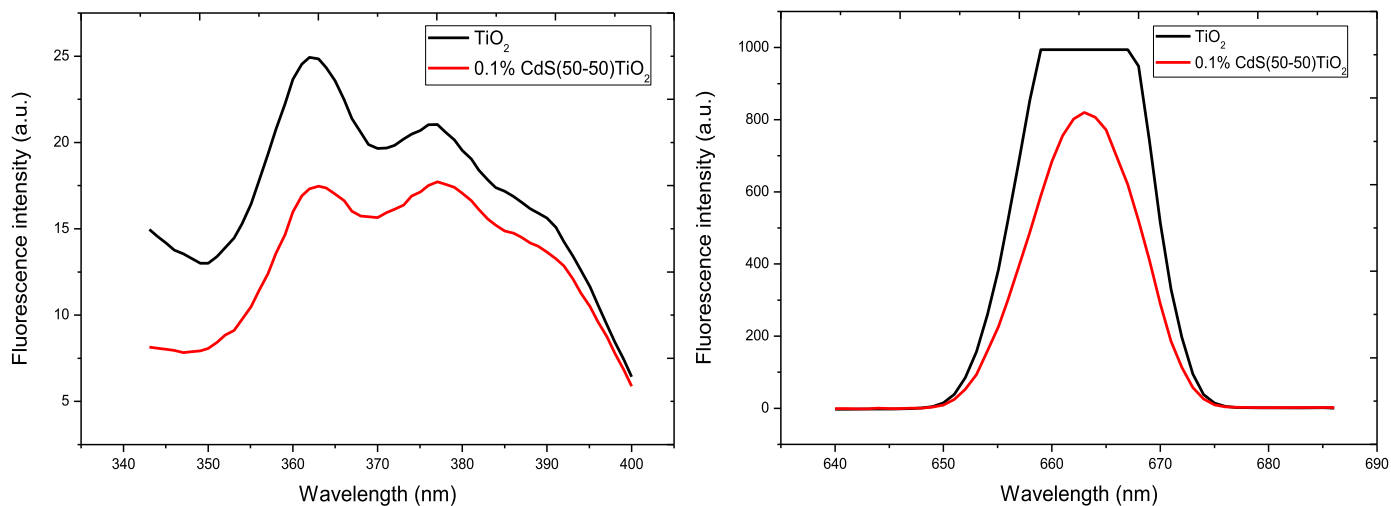
Fig. 6. Fluorescence spectrum of TiO_2 and 0.1% CdS(50-50)/TiO_2 catalysts.
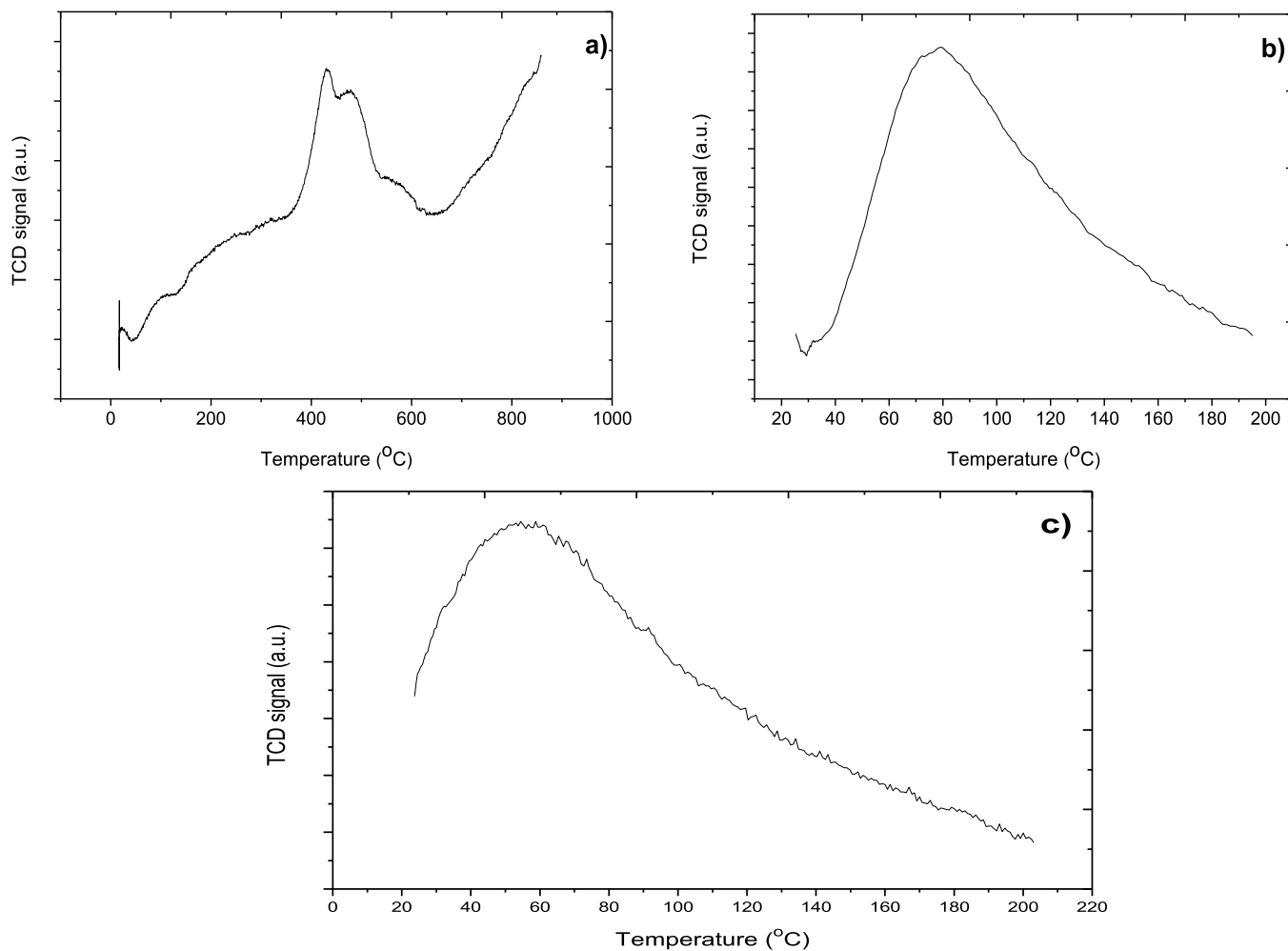
Fig. 7. H_2-TPR (a), O_2-TPO (b), and NH_3-TPD (c) profiles of 0.1% CdS(50-50)/TiO_2 catalyst.

of photo-induced electrons and holes [67]. Thus, the 0.1% CdS (50-50)/TiO_2 catalyst could effectively divide photo-induced electrons from the holes on the TiO_2 surface; thereby, making their recombination difficult and resulting in increased photocatalytic activity.

The CdS-based TiO_2 catalyst was examined by H_2-TPR analysis to investigate behavior during reduction with hydrogen and the analysis

results are shown in Fig. 7a. H_2-TPR analysis provides knowledge about the interplay between CdS and TiO_2 due to the effects on the catalytic performance and properties of the catalyst when TiO_2 interacts with the metal [68]. TiO_2 and 0.1% Cd/TiO_2 catalysts underwent TPR, TPO, and TPD analyses in our previous study [58]. TPR profiles show the reduction behavior of metal oxides in catalysts. The H_2-TPR analysis of
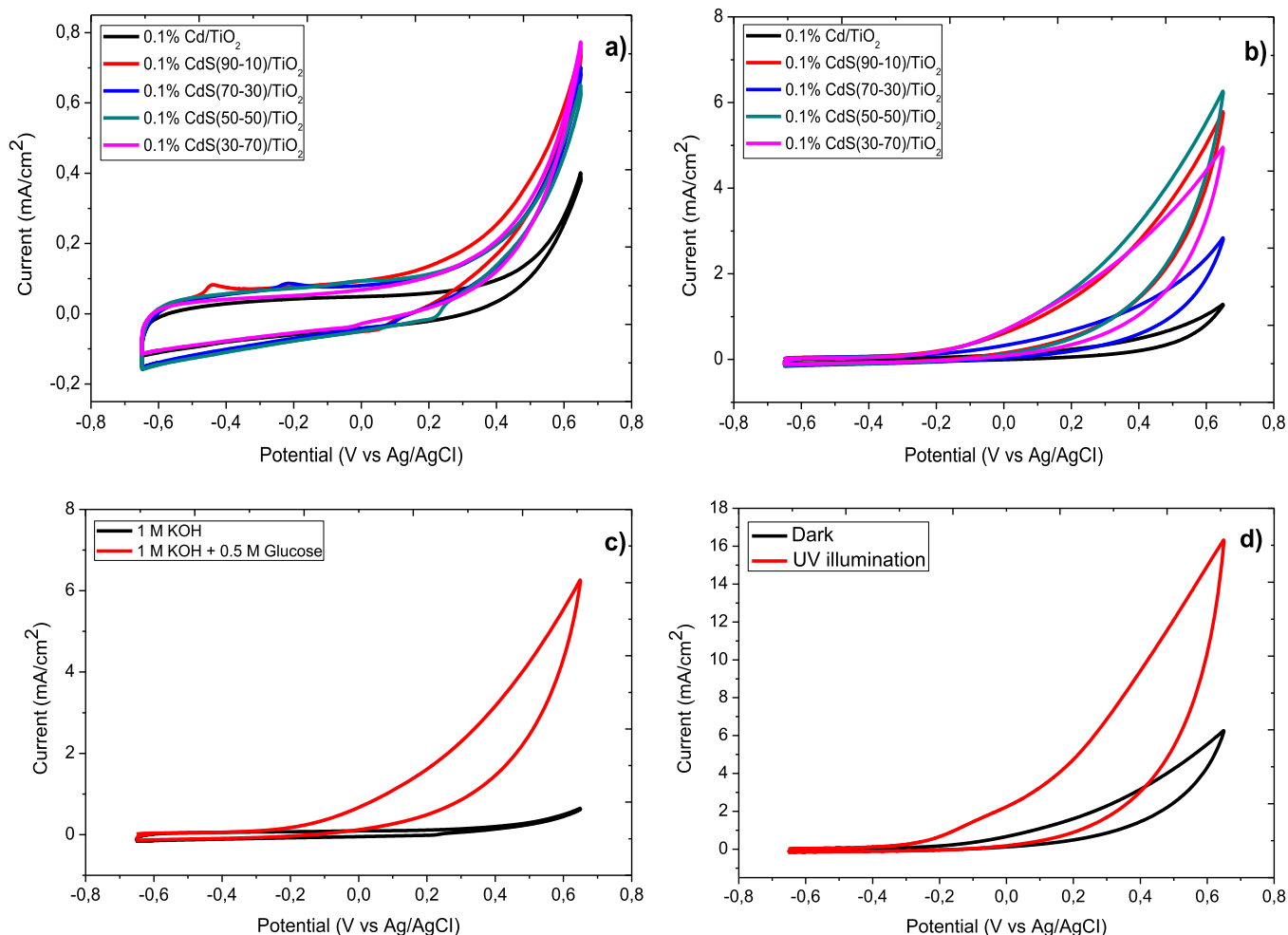
Fig. 8. Cyclic voltammograms of 0.1% CdS-based TiO₂ catalysts in (a) 1 M KOH, (b) 1 M KOH + 0.5 M $C_6H_{12}O_6$, (c) comparison KOH and $C_6H_{12}O_6$ of 0.1% CdS(50-50)/TiO₂ catalyst, (d) both dark and UV illumination of 0.1% CdS(50-50)/TiO₂ catalyst at 100 mV/s scan rate.

TiO₂ was examined by many researchers in the literature and the peak TiO₂ or Ti^{4+} reduction was obtained at approximately 400–750 °C [69]. From Fig. 7a, the 0.1% CdS-based TiO₂ catalyst has two peaks on the TPR profile at about 430 °C and 478 °C. When TiO₂ is doped with Cd or CdS metals, its reducibility increases, and therefore the reduction temperatures decrease. Fig. 7b demonstrates the O₂-TPO analysis of 0.1% CdS-based TiO₂ catalyst. TPO analysis is a material characterization process which heats a sample to a specific temperature by passing an oxidizing gas mix including oxygen over it and then leads to oxidation in the thermal excitation that occurs. In Fig. 7b, the 0.1% CdS-based TiO₂ catalyst has a sharp peak on the TPO profile at about 80 °C. When it was doped with Cd and S metals, the metals were oxidized before the support material and the oxidation temperature decreased due to the metal support contact [70]. Therefore, the much lower oxidation temperature of the CdS-based TiO₂ catalyst compared to TiO₂ can result from the formation of Cd and S alloys. TPD analysis is utilized to define the

adsorption sites on the sample with an inert mixture of gases such as NH₃ and CO₂, which examines events happening on the surface of solid samples whose temperature is modified *via* a temperature program. This analysis primarily involves measuring the rate of adsorption from the sample surface at low temperatures with a known gas and inert gas mixture, and the rate of desorption as the temperature increases [71]. The NH₃-TPD curve for the 0.1% CdS(50-50)/TiO₂ catalyst is presented in Fig. 7c. TPD curves change the acidic state of the sample as a weak, medium, and strong acid as the temperature rises [72,73]. While the peak assigned to physical adsorption for TiO₂ catalyst was found at about 50 °C, it was obtained as a wide peak at about 57 °C for CdS-based TiO₂.

3.2. Electrochemical measurements of CdS/TiO₂ catalysts

The CdS-based TiO₂ catalysts were examined by using glucose as fuel

Table 3
Electrochemical behaviors of 0.1% CdS-based TiO₂ catalysts in the dark for glucose electrooxidation.

Sample		Total current (mA/cm²)			Mass activity(mA/mg Cd)	Onset potential (V)	UV illumination CA (mA/cm²)After 1000 s
		Dark					
	KOH	Glucose	Normal				
0.1% CdS(90-10)/TiO₂	0.76	5.76	5.00		12,512.51	-0.33	0.29
0.1% CdS(70-30)/TiO₂	0.70	2.84	2.14		5360.72	-0.36	0.22
0.1% CdS(50-50)/TiO₂	0.65	6.26	5.61		14,081.33	-0.34	0.45
0.1% CdS(30-70)/TiO₂	0.77	4.94	4.17		10,509.07	-0.35	0.27
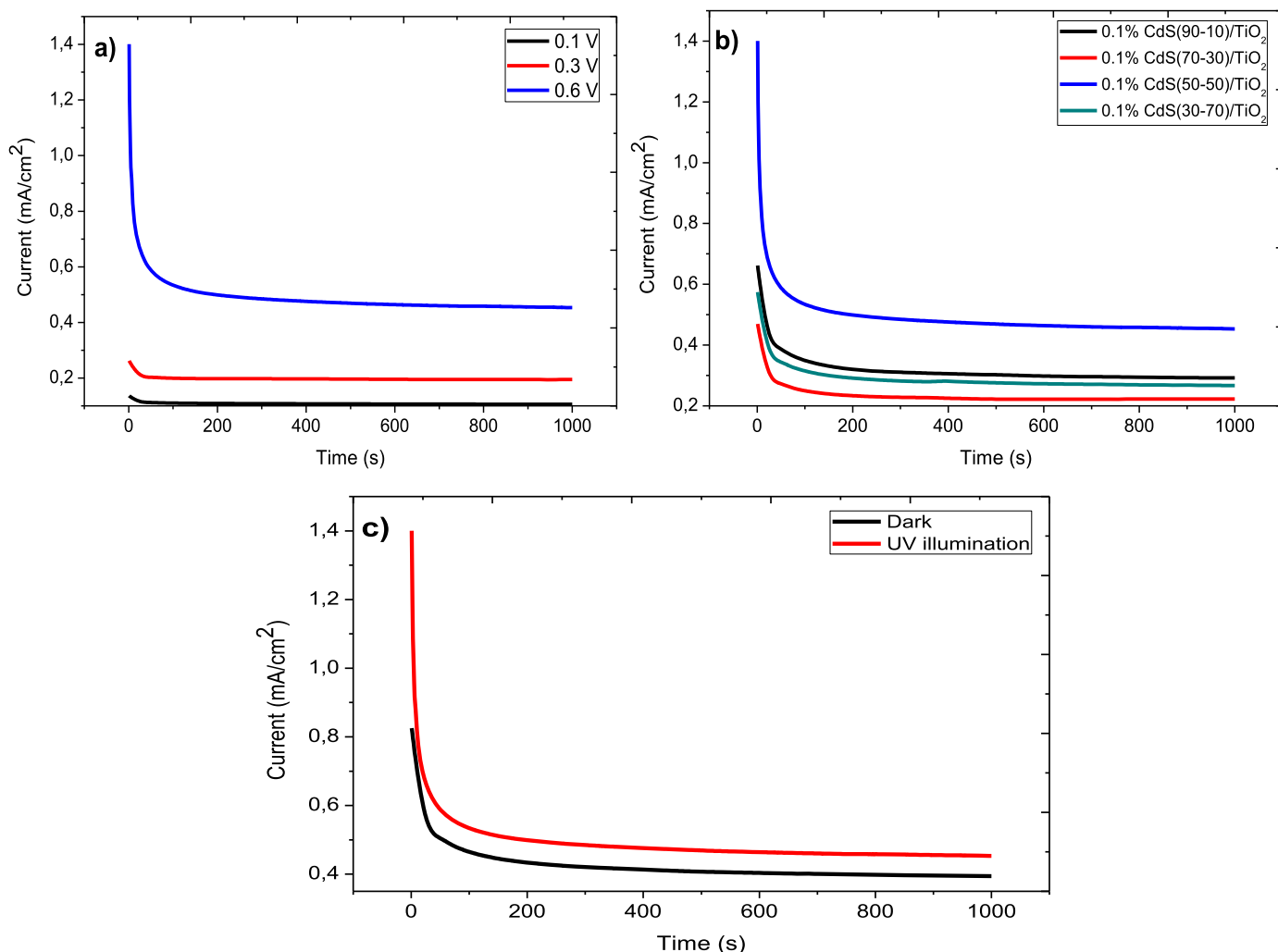
Fig. 9. CA curvesfor (a) 0.1 CdS(50-50)/TiO$_2$ under UV illumination at 0.1 V, 0.3 V, and 0.6 V potentials, (b) 0.1% CdS-based TiO$_2$ catalysts under UV illumination at 0.6 V, (c) 0.1% CdS(50-50)/TiO$_2$at both dark and UV illumination at 0.6 V in 1 M KOH + 0.5 M C$_6$H$_{12}$O$_6$ solution.

for photocatalytic performance. The CV, CA, and EIS analyses were completed to investigate the catalytic activity both in the dark and with UV illumination in 1 M KOH + 0.5 M C$_6$H$_{12}$O$_6$ solution. Fig. 8(a–d) shows the PGE of catalysts in the dark and under UV illumination. The electrochemical behaviors of 0.1% CdS-based TiO$_2$ catalysts were examined with CV analysis between -0.65 and 0.65 V potential and a scan rate of 100 mV/s in 1 M KOH and 1 M KOH + 0.5 M C$_6$H$_{12}$O$_6$ solution (Fig. 8a and b). Table 3 demonstrates the catalytic activities of the CdS-based TiO$_2$ catalysts formed at the total current values in the dark in the KOH and glucose solution. Although glucose has high energy density, it is a difficult fuel to break down. Therefore, the catalysts were evaluated according to total current because oxidation peaks did not occur in glucose electrooxidation measurements. From Fig. 8b, the 0.1% CdS(50-50)/TiO$_2$ catalyst displayed the best catalytic activity compared to the others, with specific activity at total current (glucose) of 5.61 mA/cm^2 (14081.33 mA/mg Cd) in the dark. Fig. 8c shows a comparison of 0.1% CdS(50-50)/TiO$_2$ catalyst with two solutions containing KOH and C$_6$H$_{12}$O$_6$.The specific activity (5.61 mA/cm^2) occurring between the normal total current KOH and KOH + glucose given in Table 3 shows the catalytic activity resulting from glucose. The 0.1% CdS(50-50)/TiO$_2$ catalyst was examined under UV illumination for PGE (Fig. 8d). The 0.1% CdS(50-50)/TiO$_2$ catalyst, with its low onset potential (-0.44 V, Ag/AgCl) and high catalytic activity (16.21 mA/cm^2 and 40687.75 mA/mg Cd), exhibited 3.1 times better photocurrent density than the result obtained in the dark. Furthermore, it exhibited better photocatalytic

activity under UV illumination compared to C-TNT (9.10 mA/cm^2) [74] and 0.1% Cd/TiO$_2$ (6.00 mA/cm^2) [58] among our previous studies. Though it includes a small amount of metal compared to the literature, it can be a promising anode catalyst as a photocatalyst for PFCs with high catalytic activity.

CA analysis was performed to evaluate the stability and poison resistance of CdS-based TiO$_2$ catalysts. Fig. 9(a–c) demonstrates the CA curves of catalysts. CA analysis of 0.1% CdS(50-50)/TiO$_2$ catalyst was performed at different potentials (0.1 V, 0.3, and 0.6 V) under UV illumination (Fig. 9a). CA analysis at 0.6 V potential exhibited the best resistance and stability. After 1000 s, 0.1% CdS(50-50)/TiO$_2$ catalyst had better activity and stability with 0.45 mA/cm^2 specific activity compared to other catalysts under UV illumination at 0.6 V potential (Fig. 9b). In Fig. 9c, the 0.1% CdS(50-50)/TiO$_2$ catalyst under UV illumination was more stable than in the dark (0.39 mA/cm^2). As with the CV results, 0.1% CdS(50-50)/TiO$_2$ catalyst exhibited the best activity and stability compared to analysis in the dark and at other atomic molar ratios.

Fig. 10(a–d) indicates the Nyquist plots obtained from the EIS analysis to investigate the electrocatalytic resistance of the 0.1% CdS-based TiO$_2$ catalysts. These plots are usually semicircles, where the electrocatalytic resistance increases as the diameter of the circle decreases [75,76]. The charge transfer resistance (R$_{ct}$) is associated with the diameter of the semicircle because as the diameter decreases, R$_{ct}$ decreases, and so the catalytic activity increases [77]. Fig. 10a
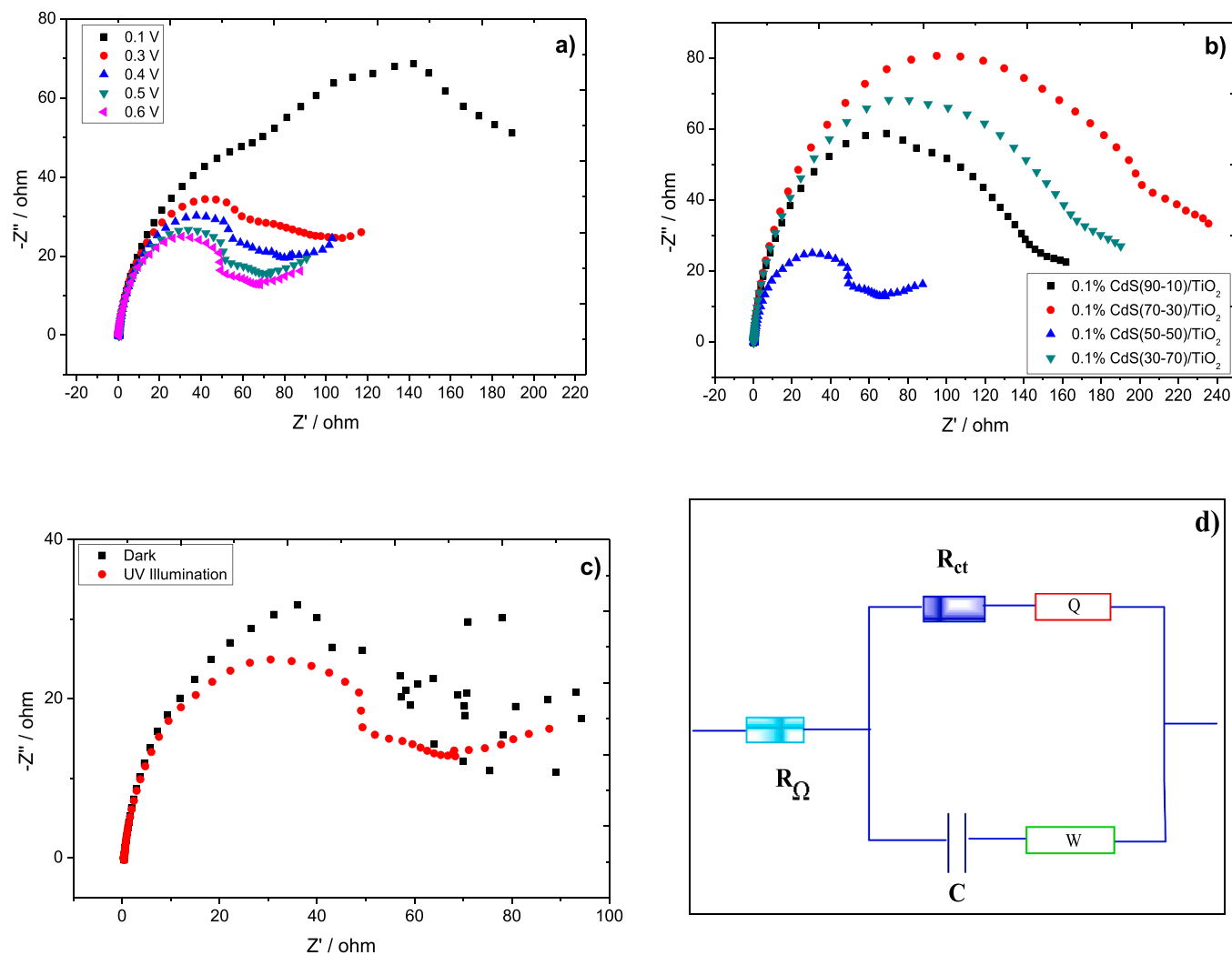
Fig. 10. Nyquist plots for (a) 0.1% CdS(50-50)/TiO$_2$ under UV illumination at 0.1 V, 0.3 V, 0.4 V, 0.5 V, and 0.6 V potentials, (b) Comparison of 0.1% CdS-based TiO$_2$ catalysts under UV illumination at 0.6 V, (c) 0.1% CdS(50-50)/TiO$_2$ catalyst in the dark and under UV illumination at 0.6 V, (d) Equivalent circuit in the dark and under UV illumination for 0.1% CdS(50-50)/TiO$_2$catalyst in 1 M KOH + 0.5 M C$_6$H$_{12}$O$_6$ solution.

Table 4
Parameters of the equivalent circuit at 0.6 V potential for photocatalytic glucose electrooxidation on 0.1% CdS(50-50)/TiO$_2$ catalyst.

0.1% CdS(50-50)/TiO$_2$	
Dark	**UV illumination**
R$_\Omega$ = 3.466 Ω	R$_\Omega$ = 3.476 Ω
R$_{ct}$ = 596.0 Ω	R$_{ct}$ = 524.6 Ω
C$_{dl}$ = 7.270 e^{-5} F	C$_{dl}$ = 7.349 e^{-5} F

demonstrates the Nyquist plots of the 0.1% CdS(50-50)/TiO$_2$ under UV illumination at different potentials (0.1 V, 0.3 V, 0.4 V, 0.5 V, and 0.6 V). As shown in Fig. 10a, the Nyquist plot taken at the potential of 0.6 V displayed the best photocatalytic activity. Fig. 10b shows the Nyquist plots for 0.1% CdS(90-10)/TiO$_2$, 0.1% CdS(70-30)/TiO$_2$, 0.1% CdS (50-50)/TiO$_2$, and 0.1% CdS(30-70)/TiO$_2$catalysts. It can clearly be seen from Fig. 10b that 0.1% CdS(50-50)/TiO$_2$ catalyst had much smaller R$_{ct}$ value compared to other atomic molar ratios. In addition, Table 4, Fig. 10c and d show the equivalent circuit resistance model and parameters, and Nyquist plot in the dark and under UV illumination for 0.1% CdS(50-50)/TiO$_2$ catalyst at 0.6 V. Fig. 10c reveals the R$_{ct}$ of 0.1% CdS(50-50)/TiO$_2$ under UV illumination is much smaller than compared to value in the dark, disclosing a notable decrease in R$_{ct}$ (524.6 Ω), indicating faster electron transfer rate and higher catalytic activity

during photocatalytic glucose electrooxidation. It can be thought that the reason why bimetallic catalysts such as 0.1% CdS-based TiO$_2$ have higher catalytic activity, stability, and resistance than monometallic catalysts provide much better activity due to the synergistic effects provided by the alloy nanostructure and higher tolerance to the poisoning effect [78]. Therefore, the slow kinetics of other atomic ratios is due to the fact that CO$_{ad}$ or CO$_2$ blocks further adsorption and dehydrogenation of glucose [79]. The CPE (constant-phase elements) specified in the circuit model are listed as R$_\Omega$ (cell ohmic resistance), R$_{ct}$ (electrochemical kinetic-related resistance), and C$_{dl}$ (double-layer capacitance corresponding to charge storage at the interface between the electrolyte and electrode) [80–82].

4. Conclusion

CdS-based TiO$_2$ catalysts were synthesized by using the WI method. The XRD, SEM-EDX, TEM, XPS, UV-VIS spectroscopy, fluorescence spectroscopy, TPR, TPO, and TPD analyses were performed to characterize the catalysts. The XRD results revealed that only anatase-TiO$_2$ structures were detected due to the use of a very low amount of CdS metal. This indicates that the metals were well dispersed in TiO$_2$ [48]. SEM-EDX and mapping and TEM-EDS results demonstrated that anatase-TiO$_2$ and CdS metal particles were formed. In addition, CdS particles had a particle size of 5.1 nm and were homogeneously dispersed. In

many studies, it has been emphasized that the particle size has an effect on the activity, and the catalytic activity increases with the decrease of the particle size [50,51]. XPS analysis illustrated that the electronic state and crystal structure of the catalyst changed. The UV-VIS spectrum showed that the bandgap of CdS-based TiO_2 decreased relative to TiO_2 but still remained in the UV region. TPR, TPO, and TPD analyses showed positive or negative shifts in the reduction, oxidation, and adsorption-desorption peaks for TiO_2 when the temperature increased when doped with metal, indicating the presence of metal. The CV, CA, and EIS analyses were performed for the activity, stability, and resistance during PGE measurements of 0.1% CdS-based TiO_2 catalysts in the dark and under UV illumination, respectively. Photocurrent measurements revealed the photoelectrochemical properties of 0.1% CdS-based TiO_2 catalysts. The 0.1% CdS(50-50)/TiO_2 catalyst exhibited the best photocatalytic activity compared to the value in the dark (5.61 mA/cm^2) and for other catalysts, with high photocurrent density (16.21 mA/cm^2) and mass (40687.75 mA/mg Cd) activity. The interface contact created between CdS and TiO_2 by the WI method results in higher photostability and improved photocurrent. Furthermore, it had the best stability and resistance for PGE according to other analyses under UV illumination, as in the CV analysis. It was observed that 0.1% CdS(50-50)/TiO_2 catalyst under UV illumination had a faster electron transfer rate and higher catalytic activity during PGE with the best stability and lowest Rct (524.6 Ω) value compared to dark (596.0 Ω). There are very few studies in the literature about photocatalytic glucose electrooxidation. They have reported PGE on C-TNT [74], Cd/TiO_2 [58], CdSe/TiO_2 [83], Cu_2O-TiO_2 [84], and anatase TiO_2 [85] photocatalysts. The 0.1% CdS (50-50)/TiO_2 catalyst has high catalytic activity forPGE and glucose electrooxidation compared to the literature. These results are promising as a photoanode catalyst for PFCs with low metal content and high specific and mass photoactivity.

CRediT authorship contribution statement

Aykut Caglar: Conceptualization, Methodology, Validation, Formal analysis, Investigation, Resources, Project administration, Data curation, Writing – original draft, Writing – review & editing, Visualization, Supervision. **Nahit Aktas:** Methodology, Validation, Formal analysis, Project administration, Funding acquisition. **Hilal Kivrak:** Conceptualization, Methodology, Validation, Formal analysis, Investigation, Resources, Project administration, Funding acquisition, Data curation, Writing – original draft, Writing – review & editing, Visualization, Supervision.

Declaration of Competing Interest

None.

Acknowledgment

References

[1] S.A. Asongu, M.O. Agboola, A.A. Alola, F.V. Bekun, The criticality of growth, urbanization, electricity and fossil fuel consumption to environment sustainability in Africa, Sci. Total Environ. 712 (2020), 136376.

[2] A. Galińska, J. Walendziewski, Photocatalytic water splitting over Pt–TiO_2 in the presence of sacrificial reagents, Energy Fuels 19 (2005) 1143–1147.

[3] Z. Ma, J. Liu, Y. Zhu, Y. Zhao, H. Lin, Y. Zhang, H. Li, J. Zhang, Y. Liu, W. Gao, S. Li, L. Li, Crystal-facet-dependent catalysis of anatase TiO2 on hydrogen storage of MgH2, J. Alloy. Compd. 822 (2020), 153553.

[4] M. Akdemir, T. Avci Hansu, A. Caglar, M. Kaya, H. Demir Kivrak, Ruthenium modified defatted spent coffee catalysts for supercapacitor and methanolysis application, Energy Storage 3 (2021) e243.

[5] P. Reeves, R. Ohlhausen, D. Sloan, K. Pamplin, T. Scoggins, C. Clark, B. Hutchinson, D. Green, Photocatalytic destruction of organic dyes in aqueous TiO2 suspensions using concentrated simulated and natural solar energy, Solar Energy 48 (1992) 413–420.

[6] S. Pinilla, A. Machín, S.H. Park, J.C. Arango, V. Nicolosi, F. Márquez -Linares, C. Morant, TiO2-based nanomaterials for the production of hydrogen and the development of lithium-ion batteries, J. Phys. Chem. B 122 (2018) 972–983.

[7] A. Caglar, T. Sahan, M.S. Cogenli, A.B. Yurtcan, N. Aktas, H. Kivrak, A novel central composite design based response surface methodology optimization study for the synthesis of Pd/CNT direct formic acid fuel cell anode catalyst, Int. J. Hydrog. Energy 43 (2018) 11002–11011.

[8] A. Eshghi, M. kheirmand, Graphene/Ni–Fe layered double hydroxide nano composites as advanced electrode materials for glucose electro oxidation, Int. J. Hydrog. Energy 42 (2017) 15064–15072.

[9] A. Caglar, H. Kivrak, Highly active carbon nanotube supported PdAu alloy catalysts for ethanol electrooxidation in alkaline environment, Int. J. Hydrog. Energy 44 (2019) 11734–11743.

[10] X. Li, G. Wang, L. Jing, W. Ni, H. Yan, C. Chen, Y.M. Yan, A photoelectrochemical methanol fuel cell based on aligned TiO2 nanorods decorated graphene photoanode, Chem. Commun. 52 (2016) 2533–2536.

[11] L. Han, S. Guo, M. Xu, S. Dong, Photoelectrochemical batteries for efficient energy recovery, Chem. Commun. 50 (2014) 13331–13333.

[12] Q. Zhao, Z. Li, Q. Deng, L. Zhu, S. Luo, H. Li, Paired photoelectrocatalytic reactions of glucose driven by a photoelectrochemical fuel cell with assistance of methylene blue, Electrochim. Acta 210 (2016) 38–44.

[13] K. Elouarzaki, A. Le Goff, M. Holzinger, J. Thery, S. Cosnier, Electrocatalytic oxidation of glucose by rhodium porphyrin-functionalized MWCNT electrodes: application to a fully molecular catalyst-based glucose/O2 fuel cell, J. Am. Chem. Soc. 134 (2012) 14078–14085.

[14] A. Caglar, B. Ulas, O. Sahin, H. Demir Kivrak, Few-layer graphene coated on indium tin oxide electrodes prepared by chemical vapor deposition and their enhanced glucose electrooxidation activity, Energy Storage 1 (2019) e73.

[15] A. Caglar, B. Ulas, O. Sahin, H. Kivrak, Synthesis of *in situ* N-, S-, and B-doped few-layer graphene by chemical vapor deposition technique and their superior glucose electrooxidation activity, Int. J. Energy Res. 43 (2019) 8204–8216.

[16] A. Caglar, D. Düzenli, I. Onal, I. Tezsevin, O. Sahin, H. Kivrak, A comparative experimental and density functional study of glucose adsorption and electrooxidation on the Au-graphene and Pt-graphene electrodes, Int. J. Hydrog. Energy 45 (2020) 490–500.

[17] A. Caglar, D. Düzenli, I. Onal, I. Tezsevin, O. Sahin, H. Kivrak, A novel experimental and density functional theory study on palladium and nitrogen doped few layer graphene surface towards glucose adsorption and electrooxidation, J. Phys. Chem. Solids 150 (2021), 109684.

[18] A. Brouzgou, S. Song, P. Tsiakaras, Carbon-supported PdSn and Pd3Sn2 anodes for glucose electrooxidation in alkaline media, Appl. Catal. B Environ. 158–159 (2014) 209–216, s.

[19] S.J. Lu, S.B. Ji, J.C. Liu, H. Li, W.S. Li, Photoelectrocatalytic oxidation of glucose at a ruthenium complex modified titanium dioxide electrode promoted by uric acid and ascorbic acid for photoelectrochemical fuel cells, J. Power Sources 273 (2015) 142–148.

[20] R. Ameta, M.S. Solanki, S. Benjamin, S.C. Ameta, Chapter 6 - photocatalysis, in: S. C. Ameta, R. Ameta (Eds.), Advanced Oxidation Processes for Waste Water Treatment, Academic Press, 2018, pp. 135–175.

[21] Y. Matsumoto, Energy positions of oxide semiconductors and photocatalysis with iron complex oxides, J. Solid State Chem. 126 (1996) 227–234.

[22] M. Song, L. Wang, J. Li, D. Sun, R. Guan, H. Zhai, X. Gao, X. Li, Z. Zhao, Z. Sun, Defect density modulation of La_2TiO_5: an effective method to suppress electron-hole recombination and improve photocatalytic nitrogen fixation, J. Colloid Interface Sci. 602 (2021) 748–755.

[23] X. Li, J. Li, H. Zhai, M. Song, L. Wang, R. Guan, Q. Zhang, Z. Zhao, Efficient catalytic fixation nitrogen activity under visible light by molybdenum doped mesoporous TiO_2, Catal. Lett. 152 (2022) 116–123.

[24] X. Gao, M. Song, D. Sun, R. Guan, H. Zhai, Z. Zhao, Q. Zhang, X. Li, A facile *in situ* hydrothermal etching method to $CaTiO_3$/TiO_2 heterostructure for efficient photocatalytic N2 reduction, Catal. Lett. 152 (2022) 1990–1998.

[25] M. Li, J. Zhang, L. Wang, X. Cheng, X. Gao, Y. Wang, G. Zhang, Y. Qi, H. Zhai, R. Guan, Direct Z-scheme oxygen-vacancy-rich TiO_2/Ta_3N_5 heterojunction for degradation of ciprofloxacin under visible light: degradation pathways and mechanism insight, Appl. Surf. Sci. 583 (2022), 152516.

[26] S. Nishanthi, D.H. Raja, E. Subramanian, D.P. Padiyan, Remarkable role of annealing time on anatase phase titania nanotubes and its photoelectrochemical response, Electrochim. Acta 89 (2013) 239–245.

[27] A. Fujishima, K. Honda, Electrochemical photolysis of water at a semiconductor electrode, Nature 238 (1972) 37–38.

[28] G.L. Chiarello, M.V. Dozzi, E. Selli, TiO_2-based materials for photocatalytic hydrogen production, J. Energy Chem. 26 (2017) 250–258.

[29] L. Zheng, F. Teng, X. Ye, H. Zheng, X. Fang, Photo/electrochemical applications of metal sulfide/TiO_2 heterostructures, Adv. Energy Mater. 10 (2020), 1902355.

[30] B. Pan, Q. Pin, C. Wang, 6 - Photoreduction of CO2 on non-TiO_2–based metal oxides, in: X. Wang, M. Anpo, X. Fu (Eds.), Current Developments in Photocatalysis and Photocatalytic Materials, Elsevier, 2020, pp. 77–87.

[31] A.T. Kuvarega, B.B. Mamba, TiO_2-based photocatalysis: toward visible light-responsive photocatalysts through doping and fabrication of carbon-based nanocomposites, Crit. Rev. Solid State Mater. Sci. 42 (2017) 295–346.

[32] C. Hu, D. Kelm, M. Schreiner, T. Wollborn, L. Mädler, W.Y. Teoh, Designing photoelectrodes for photocatalytic fuel cells and elucidating the effects of organic substrates, ChemSusChem 8 (2015) 4005–4015.

[33] H. Kivrak, D.İ. Saleh, D. Alpaslan, A. Çağlar, K. Selçuk, T.E. Dudu, N. Aktas, Quantum size effect of cadmium-doped titanium dioxide photocatalysts towards methylene blue degradation and electrooxidation, Int. J. Environ. Sci. Technol. (2021) 1–12.

[34] O. Ozok-Arici, S. Kaya, A. Caglar, H. Kivrak, A. Kivrak, Glucose electrooxidation study on 3-iodo-2-(aryl/alkyl)benzo[b]thiophene organic catalyst, J. Electron. Mater. 51 (2022) 1653–1662.

[35] D. Chu, X.H. Li, D.X. Feng, J.S. Gu, G. Shen, Electrocatalytic oxidation of glucose on carbon nanotube/nanocrystalline TiO₂ film loaded Pt complex electrode, Acta Chim. Sin. 62 (2004) 2403–2406.

[36] Y. Gu, H. Yang, B. Li, J. Mao, Y. An, A ternary nanooxide NiO-TiO₂-ZrO₂/SO₄²⁻ as efficient solid superacid catalysts for electro-oxidation of glucose, Electrochim. Acta 194 (2016) 367–376.

[37] M. Long, L. Tan, A.D. Tang, The effects of electroplating conditions on the morphology and glucose oxidation performance of Cu₂O/TiO₂, Adv. Mater. Res. 937 (2014) 3–8.

[38] Y. Gu, Y. Liu, H. Yang, B. Li, Y. An, Electrocatalytic glucose oxidation *via* hybrid nanomaterial catalyst of multi-wall TiO₂ nanotubes supported Ni(OH)₂ nanoparticles: optimization of the loading level, Electrochim. Acta 160 (2015) 263–270.

[39] T.N.Q. Trang, N.D. Nam, L.T. Ngoc Tu, H.P. Quoc, T. Van Man, V.T.T. Ho, V.T. H. Thu, *In situ* spatial charge separation of an Ir@TiO₂ multiphase photosystem toward highly efficient photocatalytic performance of hydrogen production, J. Phys. Chem. C 124 (2020) 16961–16974.

[40] Z. Xiong, Z. Lei, Y. Li, L. Dong, Y. Zhao, J. Zhang, A review on modification of facet-engineered TiO2 for photocatalytic CO₂ reduction, J. Photochem. Photobiol. C Photochem. Rev. 36 (2018) 24–47.

[41] E. Antolini, Structural parameters of supported fuel cell catalysts: the effect of particle size, inter-particle distance and metal loading on catalytic activity and fuel cell performance, Appl. Catal. B Environ. 181 (2016) 298–313.

[42] E. Antolini, Carbon supports for low-temperature fuel cell catalysts, Appl. Catal. B Environ. 88 (2009) 1–24.

[43] N.M. Deraz, The comparative jurisprudence of catalysts preparation methods: I. Precipitation and impregnation methods, J. Ind. Environ. Chem 2 (2018) 19–21.

[44] B. Tavakoli, S. Eskandari, U. Khan, R. White, J. Regalbuto, A review of preparation methods for supported metal catalysts 61 (2017) 1–35.

[45] W. Li, M. Zhang, Z. Du, Q. Ma, H. Jameel, H.M. Chang, Photocatalytic degradation of lignin model compounds and kraft pine lignin by CdS/TiO₂ under visible light irradiation, BioResources 10 (2015) 1245–1259.

[46] R. Guan, D. Wang, Y. Zhang, C. Liu, W. Xu, J. Wang, Z. Zhao, M. Feng, Q. Shang, Z. Sun, Enhanced photocatalytic N2 fixation *via* defective and fluoride modified TiO₂ surface, Appl. Catal. B Environ. 282 (2021), 119580.

[47] X. Qu, M. Liu, L. Li, R. Wang, H. Sun, L. Shi, F. Du, BiOBr flakes decoration and structural modification for CdTe/TiO₂ spheres: towards water decontamination under simulated light irradiation, Mater. Sci. Semicond. Process. 93 (2019) 331–338.

[48] K. Huang, L. Chen, J. Deng, J. Xiong, Enhanced visible-light photocatalytic performance of nanosized anatase TiO₂ doped with CdS quantum dots for cancer-cell treatment, J. Nanomater. 2012 (2012), 720491.

[49] H. Gholap, R. Patil, P. Yadav, A. Banpurkar, S. Ogale, W. Gade, CdTe-TiO2 nanocomposite: an impeder of bacterial growth and biofilm, Nanotechnology 24 (2013), 195101.

[50] D.S. Kim, S.J. Han, S.Y. Kwak, Synthesis and photocatalytic activity of mesoporous TiO₂ with the surface area, crystallite size, and pore size, J. Colloid Interface Sci. 316 (2007) 85–91.

[51] C. Jiang, M. Wei, Z. Qi, T. Kudo, I. Honma, H. Zhou, Particle size dependence of the lithium storage capability and high rate performance of nanocrystalline anatase TiO2 electrode, J. Power Sources 166 (2007) 239–243.

[52] C.L. Chiang, J.M. Yang, Flame retardance and thermal stability of polymer/graphene nanosheet oxide composites, in: D.Y. Wang (Ed.), Novel Fire Retardant Polymers and Composite Materials, Woodhead Publishing, 2017, pp. 295–312.

[53] C. Kumar, A. Pattammattel. Characterization techniques for graphene, Introduction to Graphene, Elsevier, 2017, pp. 45–74.

[54] B. Bharti, S. Kumar, H.N. Lee, R. Kumar, Formation of oxygen vacancies and Ti³⁺ state in TiO₂ thin film and enhanced optical properties by air plasma treatment, Sci. Rep. 6 (2016) 1–12.

[55] W. Li, M. Li, S. Xie, T. Zhai, M. Yu, C. Liang, X. Ouyang, X. Lu, H. Li, Y. Tong, Improving the photoelectrochemical and photocatalytic performance of CdO nanorods with CdS decoration, CrystEngComm 15 (2013) 4212–4216.

[56] Y.S. Li, F.L. Jiang, Q. Xiao, R. Li, K. Li, M.F. Zhang, A.Q. Zhang, S.F. Sun, Y. Liu, Enhanced photocatalytic activities of TiO₂ nanocomposites doped with water-soluble mercapto-capped CdTe quantum dots, Appl. Catal. B Environ. 101 (2010) 118–129.

[57] G. Yang, B. Yang, T. Xiao, Z. Yan, One-step solvothermal synthesis of hierarchically porous nanostructured CdS/TiO₂ heterojunction with higher visible light photocatalytic activity, Appl. Surf. Sci. 283 (2013) 402–410.

[58] A. Caglar, H. Kivrak, Tailoring cadmium composition on titanium dioxide to achieve enhanced photocatalytic glucose fuel cell anode performance, ACS Appl. Energy Mater. 4 (2021) 12298–12309.

[59] B. Li, L. Jiang, X. Li, P. Ran, P. Zuo, A. Wang, L. Qu, Y. Zhao, Z. Cheng, Y. Lu, Preparation of monolayer MoS2 quantum dots using temporally shaped femtosecond laser ablation of bulk MoS2 targets in water, Sci. Rep. 7 (2017) 11182.

[60] W. Xie, R. Li, Q. Xu, Enhanced photocatalytic activity of Se-doped TiO₂ under visible light irradiation, Sci. Rep. 8 (2018) 1–10.

[61] B. Bharti, S. Kumar, H.N. Lee, R. Kumar, Formation of oxygen vacancies and Ti³⁺ state in TiO₂ thin film and enhanced optical properties by air plasma treatment, Sci. Rep. 6 (2016) 32355.

[62] J. Yu, C. Gong, Z. Wu, Y. Wu, W. Xiao, Y. Su, L. Sun, C. Lin, Efficient visible light-induced photoelectrocatalytic hydrogen production using CdS sensitized TiO₂ nanorods on TiO₂ nanotube arrays, J. Mater. Chem. A 3 (2015) 22218–22226.

[63] W. Li, M. li, S. Xie, T. Zhai, M. Yu, C. Liang, X. Ouyang, X. Lu, H. Li, Y. Tong, Improving the photoelectrochemical and photocatalytic performance of CdO nanorods with CdS decoration, CrystEngComm 15 (2013) 4212–4216.

[64] Y.S. Li, F.L. Jiang, Q. Xiao, R. Li, K. Li, M.F. Zhang, A.Q. Zhang, S.F. Sun, Y. Liu, Enhanced photocatalytic activities of TiO₂ nanocomposites doped with water-soluble mercapto-capped CdTe quantum dots, Appl. Catal. B Environ. 101 (2010) 118–129.

[65] H. Ge, F. Xu, B. Cheng, J. Yu, W. Ho, S-scheme heterojunction TiO2/CdS nanocomposite nanofiber as H2-production photocatalyst, ChemCatChem 11 (2019) 6301–6309.

[66] K. Huang, L. Chen, J. Deng, J. Xiong, Enhanced visible-light photocatalytic performance of nanosized anatase TiO2 doped with CdS quantum dots for cancer-cell treatment, J. Nanomater. 2012 (2012).

[67] J. Liqiang, Q. Yichun, W. Baiqi, L. Shudan, J. Baojiang, Y. Libin, F. Wei, F. Honggang, S. Jiazhong, Review of photoluminescence performance of nano-sized semiconductor materials and its relationships with photocatalytic activity, Solar Energy Mater. Solar Cells 90 (2006) 1773–1787.

[68] V.G. Deshmane, S.L. Owen, R.Y. Abrokwah, D. Kuila, Mesoporous nanocrystalline TiO2 supported metal (Cu, Co, Ni, Pd, Zn, and Sn) catalysts: effect of metal-support interactions on steam reforming of methanol, J. Mol. Catal. A Chem. 408 (2015) 202–213.

[69] N. Zhang, Z. Yang, Z. Chen, L. Yunxiang, Y. Liao, Y. Li, M. Gong, Y. Chen, Synthesis of sulfur-resistant TiO2-CeO2 composite and its catalytic performance in the oxidation of a soluble organic fraction from diesel exhaust, Catalysts 8 (2018) 246.

[70] J. Van Doorn, M.A. Vuurman, P. Tromp, D. Stufkens, J. Moulijn, Correlation between Raman spectroscopic data and the temperature-programmed oxidation reactivity of coals and carbons, Fuel Process. Technol. 24 (1990) 407–413.

[71] P.J. Barrie, Analysis of temperature programmed desorption (TPD) data for the characterisation of catalysts containing a distribution of adsorption sites, Phys. Chem. Chem. Phys. 10 (2008) 1688–1696.

[72] M. Zhou, P. Liu, K. Wang, J. Xu, J. Jiang, Catalytic hydrogenation and one step hydrogenation-esterification to remove acetic acid for bio-oil upgrading: model reaction study, Catal. Sci. Technol. 6 (2016) 7783–7792.

[73] H.J. Choi, J.S. Kim, M. Kang, Photodecomposition of concentrated ammonia over nanometer-sized TiO∼ 2, V-TiO∼ 2, and Pt/V-TiO∼ 2 photocatalysts, Korean Chem. Soc. 28 (2007) 581–588.

[74] A. Caglar, H. Kivrak, N. Aktas, A.O. Solak, Fabrication of carbon-doped titanium dioxide nanotubes as anode materials for photocatalytic glucose fuel cells, J. Electron. Mater. 50 (2021) 2242–2253.

[75] T.A. Hansu, A. Caglar, O. Sahin, H. Kivrak, Hydrolysis and electrooxidation of sodium borohydride on novel CNT supported CoBi fuel cell catalyst, Mater. Chem. Phys. 239 (2020), 122031.

[76] A. Caglar, M.S. Cogenli, A.B. Yurtcan, H. Kivrak, Effective carbon nanotube supported metal (M=Au, Ag, Co, Mn, Ni, V, Zn) core Pd shell bimetallic anode catalysts for formic acid fuel cells, Renew. Energy 150 (2020) 78–90.

[77] B. Ulas, A. Caglar, O. Sahin, H. Kivrak, Composition dependent activity of PdAgNi alloy catalysts for formic acid electrooxidation, J. Colloid Interface Sci. 532 (2018) 47–57.

[78] A. Caglar, B. Ulas, M.S. Cogenli, A.B. Yurtcan, H. Kivrak, Synthesis and characterization of Co, Zn, Mn, V modified Pd formic acid fuel cell anode catalysts, J. Electroanal. Chem. 850 (2019), 113402.

[79] O. Sahin, H. Kivrak, A comparative study of electrochemical methods on Pt–Ru DMFC anode catalysts: the effect of Ru addition, Int. J. Hydrog. Energy 38 (2013) 901–909.

[80] H. Liu, M.G. George, N. Ge, D. Muirhead, P. Shrestha, J. Lee, R. Banerjee, R. Zeis, M. Messerschmidt, J. Scholta, Microporous layer degradation in polymer electrolyte membrane fuel cells, J. Electrochem. Soc. 165 (2018) F3271.

[81] J. Liu, Y. Xie, Y. Nan, G. Gou, X. Li, Y. Fang, X. Wang, Y. Tang, H. Yang, J. Ma, ZnCo2O4 nanoparticles derived from dual-metal-organic-frameworks embedded in Multiwalled Carbon Nanotubes: a favorable electrocatalyst for the water splitting, Electrochim. Acta 257 (2017) 233–242.

[82] A.R. Hamad, H. Calis, A. Caglar, H. Kivrak, A. Kivrak, Indole-based novel organic anode catalyst for glucose electrooxidation, Int. J. Energy Res. 46 (2021) 1659–1671.

[83] A. Caglar, H. Kivrak, N. Aktas, The effect of titanium dioxide-supported CdSe photocatalysts enhanced for photocatalytic glucose electrooxidation under UV illumination, Int. J. Hydrog. Energy 47 (2022) 21130–21145.

[84] A. Devadoss, P. Sudhagar, C. Ravidhas, R. Hishinuma, C. Terashima, K. Nakata, T. Kondo, I. Shitanda, M. Yuasa, A. Fujishima, Simultaneous glucose sensing and biohydrogen evolution from direct photoelectrocatalytic glucose oxidation on robust Cu2O–TiO2 electrodes, Phys. Chem. Chem. Phys. 16 (2014) 21237–21242.

[85] Y. Yan, J. Fang, Z. Yang, J. Qiao, Z. Wang, Q. Yu, K. Sun, Photoelectrochemical oxidation of glucose for sensing and fuel cell applications, Chem. Commun. 49 (2013) 8632–8634.